

Chemotherapy of Skull Base Chordoma Tailored on Responsiveness of Patient-Derived Tumor Cells to Rapamycin^{1,2}

Lucia Ricci-Vitiani*, Daniele Runci*, Quintino Giorgio D'Alessandris[†], Tonia Cenci[‡], Maurizio Martini[‡], Federico Bianchi[†], Giulio Maira[†], Louis Stancato[§], Ruggero De Maria[¶], Luigi Maria Larocca^{‡,3} and Roberto Pallini^{†,3}

*Department of Haematology, Oncology and Molecular Medicine, Istituto Superiore di Sanità, Rome, Italy; [†]Institute of Neurosurgery, Università Cattolica del Sacro Cuore, Rome, Italy; [‡]Institute of Pathology, Università Cattolica del Sacro Cuore, Rome, Italy; [§]Cancer Biology and Patient Tailoring, Oncology Research, Eli Lilly and Company, Indianapolis, IN; [¶]Regina Elena National Cancer Institute, Rome, Italy

Abstract

Skull base chordomas are challenging tumors due to their deep surgical location and resistance to conventional radiotherapy. Chemotherapy plays a marginal role in the treatment of chordoma resulting from lack of preclinical models due to the difficulty in establishing tumor cell lines and valuable *in vivo* models. Here, we established a cell line from a recurrent clival chordoma. Cells were cultured for more than 30 passages and the expression of the chordoma cell marker brachyury was monitored using both immunohistochemistry and Western blot. Sensitivity of chordoma cells to the inhibition of specific signaling pathways was assessed through testing of a commercially available small molecule kinase inhibitor library. *In vivo* tumorigenicity was evaluated by grafting chordoma cells onto immunocompromised mice and established tumor xenografts were treated with rapamycin. Rapamycin was administered to the donor patient and its efficacy was assessed on follow-up neuroimaging. Chordoma cells maintained brachyury expression at late passages and generated xenografts closely mimicking the histology and phenotype of the parental tumor. Rapamycin was identified as an inhibitor of chordoma cell proliferation. Molecular analyses on tumor cells showed activation of the mammalian target of rapamycin signaling pathway and mutation of *KRAS* gene. Rapamycin was also effective in reducing the growth of chordoma xenografts. On the basis of these results, our patient received rapamycin therapy with about six-fold reduction of the tumor growth rate upon 10-month follow-up neuroimaging. This is the first case of chordoma in whom chemotherapy was tailored on the basis of the sensitivity of patient-derived tumor cells.

Neoplasia (2013) 15, 773–782

Abbreviations: MR, magnetic resonance; mTOR, mammalian target of rapamycin; PTEN, phosphatase and tensin homolog

Address all correspondence to: Roberto Pallini, MD, PhD, Institute of Neurosurgery, Università Cattolica del Sacro Cuore, Largo F. Vito, 1, 00168 Rome, Italy. E-mail: pallini@rm.unicatt.it or Lucia Ricci-Vitiani, PhD, Department of Haematology, Oncology and Molecular Medicine, Istituto Superiore di Sanità, Viale Regina Elena, 299, 00161 Rome, Italy. E-mail: lriccivitiani@yahoo.it

¹This work was supported by Fondi d'Ateneo, Linea D1, to R.P. and L.M.L. and by Associazione Italiana per la Ricerca sul Cancro (Start-up 6326) to L.R.-V. The authors declare no actual, potential, or perceived conflict of interest with regard to the manuscript submitted for review.

²This article refers to supplementary materials, which are designated by Tables W1 and W2 and Figures W1 to W5 and are available online at www.neoplasia.com.

³These authors shared senior authorship.

Received 9 January 2013; Revised 5 April 2013; Accepted 11 April 2013

Introduction

Chordomas of the skull base are biologically aggressive tumors due to their propensity to infiltrate the bone and dura mater. Current treatment consists of extensive surgical resection followed by high-dose radiation therapy. Even after appropriate treatment, however, skull base chordomas recur by 29 to 43 months after initial surgery with 5-year progression-free survival ranging from 23% to 65% and median overall survival of 6 years [1–7]. Chemotherapy plays only a marginal role in the treatment of chordomas and this is largely related to the lack of preclinical data due to the difficulty in establishing tumor cell lines and relevant *in vivo* models. In a previous study, we were able to derive long-term cell cultures from skull base chordomas showing telomerase enzyme activity [8]. More recently, Siu et al. established the first primary tumor xenograft model from a chordoma of the clivus that had recurred following radiotherapy [9]. A few cell lines have been isolated from sacral and extra-axial chordomas [10–16], three of which were demonstrated to be tumorigenic after being grafted in immunocompromised mice [14–16]. Further studies on sacral chordoma cells have shown activation of the phosphoinositide 3-kinase (PI3K)/Akt/mammalian target of rapamycin (mTOR) pathway and intrinsic stem-like properties, including potential toward osteogenic differentiation [17,18]. Here, we have established a novel cell line from a patient suffering from a recurrent chordoma of the skull base. This cell line maintained the expression of brachyury, a chordoma cell marker, at late passages in culture and generated tumor xenografts closely mimicking the histology and phenotype of parent tumor. *In vitro* screening with a library of commercially available kinase inhibitors selected for specific pathway inhibition and/or cytotoxic activity demonstrated sensitivity of the chordoma cells to rapamycin. Importantly, rapamycin was also effective in reducing the growth of chordoma tumor xenografts. On the basis of these results, our patient received rapamycin therapy leading to a substantial reduction of the tumor growth rate upon follow-up magnetic resonance (MR) images. This is the first chordoma case in which chemotherapy was tailored on the basis of the sensitivity of patient-derived tumor cells to specific small molecule inhibitors.

Materials and Methods

Patient Information and Clinical Material

Tumor tissue was obtained from a 30-year-old female patient with recurrent chordoma of the skull base. The patient had undergone a first surgery 3 years before admission with partial tumor resection through a transoral approach followed by craniocervical fixation. Further surgery and neoadjuvant treatments were refused by the patient. On MR image follow-up, the chordoma showed a slow growth for about 2 years, followed by accelerated growth with a tumor doubling time that decreased from 40.1 to 7.4 months [4] (Figure 1, A and B). Upon admission, the patient presented with cachexia, respiratory insufficiency, left-sided paresis, midline and right hemispheric cerebellar syndrome, and palsy of cranial nerves from V to XII on the right. MR images demonstrated a huge mass lesion involving the clivus, sphenoid region, right petrous bone, and temporal fossa with severe brain stem compression. Tracheostomy and gastrostomy were performed. The patient underwent a two-stage surgery through subtemporal/infratemporal and retrosigmoid approaches with extensive tumor resection and decompression of the temporal lobe and brain stem. Postoperatively, the patient's neurologic conditions improved remarkably. Gastrostomy was closed before discharge and tracheostomy 1 month later.

Tumor tissue was taken for establishment of cell cultures at the first staged surgical procedure. The patient provided informed consent. Histologic examination of surgical specimens from both procedures revealed a typical chordoma with physaliphorous cells embedded in a mucoid or chondroid matrix (Figure 1C). The tumor expressed brachyury (H-210, rabbit polyclonal antibody; Santa Cruz Biotechnology Inc, Santa Cruz, CA), epithelial membrane antigen (EMA; clone E29; Dako, Glostrup, Denmark), vimentin (clone V9; Dako), cytokeratin (clone AE1 + AE2; Dako), and S-100 (rabbit polyclonal antibody; Dako). The proliferation rate, as determined by immunostaining with anti-Ki-67 antibody (clone MIB-1; Dako), was between 5% and 8%. Phosphatase and tensin homolog (PTEN), studied with a mouse monoclonal antibody (clone 28H6; Novocastra Ltd, Newcastle, United Kingdom), was not expressed in approximately 70% of the tumor cell (Figure 1C).

Cell Cultures

Immediately after surgical removal, chordoma tissue samples were mechanically dissociated. Cells were cultured in Dulbecco's modified Eagle's medium-F12 (1:1; Gibco, Milan, Italy) supplemented with 10% FBS, 2 mM L-glutamine, 100 U/ml penicillin, and 100 µg/ml streptomycin (Gibco), in the presence of human recombinant epidermal growth factor (40 ng/ml) and human recombinant basic fibroblast growth factor (20 ng/ml; PeproTech, Inc, Rocky Hill, NJ) [8]. Adherent cells were grown to 80% confluence, detached from the flask with trypsin/EDTA (0.25% trypsin; Gibco), and replated at a density of 20×10^3 /ml in 75-cm² tissue culture flasks. The cells were replated every 4 days, corresponding to approximately two population doublings. For growth curve analysis, cells were plated at a density of 2×10^4 /ml in 96-well plates in triplicate. Cell proliferation was monitored by counting the cells and confirmed by using the CellTiter-Blue viability assay (Promega, Madison, WI).

Immunocytochemical Staining of Cultured Chordoma Cells

For immunostaining, cultured cells were plated onto polylysine-coated glass coverslips. Cells were then fixed with 4% paraformaldehyde and stained with the aforementioned antibodies. After methanol and H₂O₂ permeabilization, cells were incubated at room temperature for 1 hour with anti-brachyury antibody at 1:50. The primary antibodies were visualized using the avidin-biotin-peroxidase complex method (UltraTek HRP Anti-polyvalent; ScyTek, Logan, UT) according to the instruction manual. 3,3'-Diaminobenzidine was used as the enzyme substrate to observe the specific antibody localization, and Mayer hematoxylin was used as a nuclear counterstain.

In Vitro Small Molecule Testing

Cells were plated at a density of 2×10^4 /ml in a 96-well plate in triplicate. Twenty-four hours after seeding, cells were treated with 80 kinase inhibitors that belong to a commercial chemical library (Enzo Life Sciences/Biomol, Lausen, Switzerland; <http://www.enzolifesciences.com/BML-2832/kinase-inhibitor-library>) at 5 µM concentration (Table W1). After 48, 72, and 96 hours of treatment, cell viability was assessed using CellTiter-Glo assay (Promega, Milan, Italy) following the manufacturer's instructions. Titration experiments were performed using serial dilution of the selected compounds.

Western Blot Analysis

Cell pellets were washed twice with cold phosphate-buffered saline (PBS) and resuspended in a 50 mM Tris-HCl (pH 7.5), 200 mM

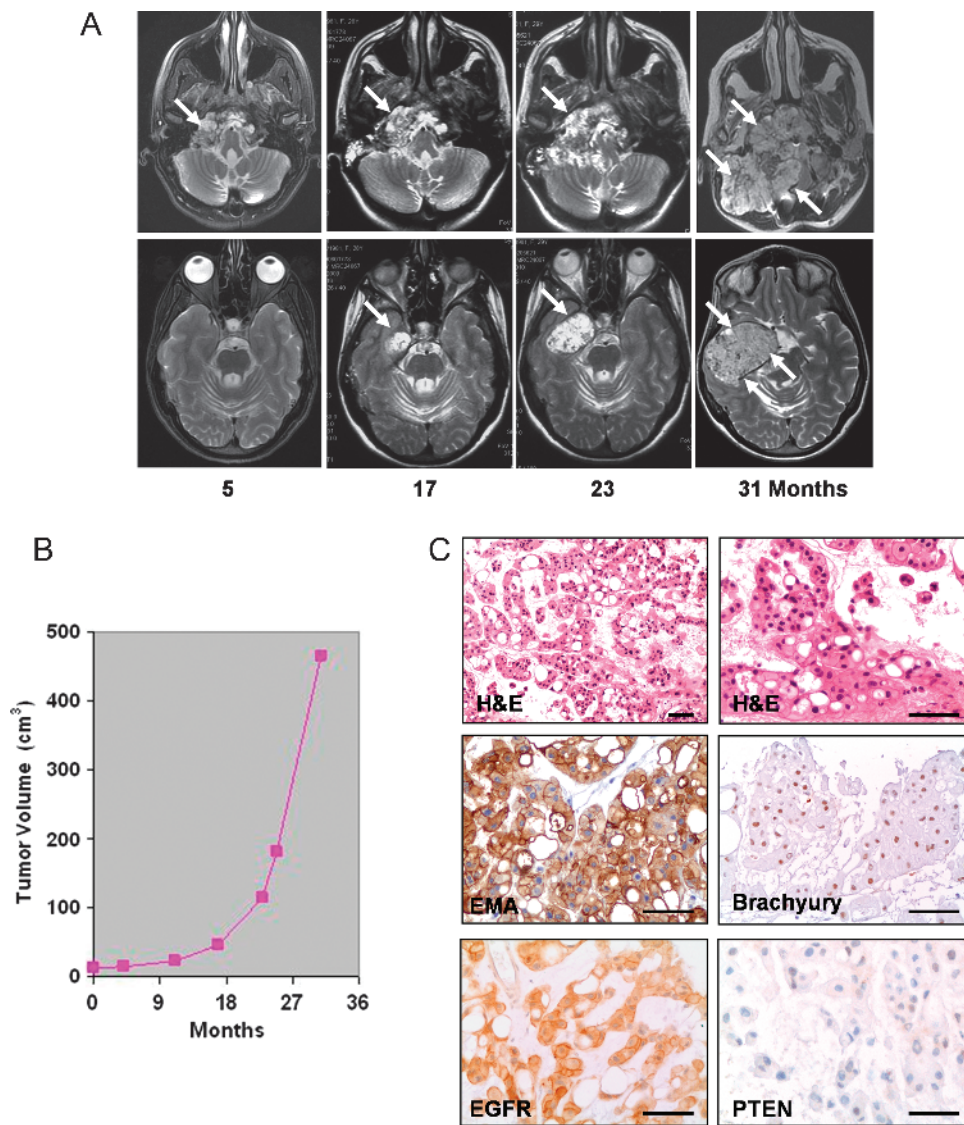


Figure 1. (A) Follow-up T2-weighted axial MR images showing the skull base chordoma, which appears as an inhomogeneous hyperintense mass lesion (arrows) involving the right petroclival area, petrous bone, sphenoid region, and middle cranial fossa. Upper panel: MR images at the level of petroclival junction. Lower panel: MR images at the level of middle cranial fossa. (B) Growth curve of clival chordoma as assessed on follow-up MR images. (C) Typical histologic appearance of chordoma with large clusters of physaliferous cells that stain positive for EMA and brachyury, with a strong membranous expression of EGFR. There is loss of PTEN expression. Scale bars, 120 μ m.

NaCl, and 1% NP-40 ice-cold buffer containing Proteinase Inhibitor Cocktail (Sigma, St Louis, MO) and incubated for 30 minutes on ice. After centrifugation at 10,000g for 10 minutes, lysates were collected as supernatants. For each sample, 20 μ g of cell extracts were resolved on a 4% to 12% sodium dodecyl sulfate–polyacrylamide gel using a mini-gel apparatus (Bio-Rad Laboratories, Richmond, CA) and transferred to Hybond-C extra nitrocellulose (Amersham Pharmacia Biotech, Piscataway, NJ). Membrane was blocked for 1 hour with 5% nonfat dry milk in TBS containing 0.05% Tween-20 and incubated overnight with primary antibody. The following primary antibodies were used: mouse anti- β -actin (Oncogene Research Products, La Jolla, CA), rabbit anti-brachyury (Santa Cruz Biotechnology Inc), mouse monoclonal anti-brachyury (5H8; Novus Biologicals, Littleton, CO), rabbit anti-mTOR, rabbit anti-phospho-mTOR (Ser²⁴⁴⁸), rabbit anti-Akt, rabbit anti-phospho-Akt (Ser⁴⁷³), rabbit anti-tuberin/tuberous sclerosis complex protein 2 (TSC2), rab-

bit anti-phospho-tuberin/TSC2 (Thr¹⁴⁶²), rabbit anti-p70 S6, and rabbit anti-phospho-p70 S6 kinase (p70 S6K, Thr³⁸⁹; all from Cell Signaling Technology, Danvers, MA). Washed filters were then incubated for 45 minutes with HRP-conjugated anti-rabbit or anti-mouse secondary antibodies (Amersham Pharmacia Biotech) and visualized by using an enhanced chemiluminescence detection system (SuperSignal West Pico Chemiluminescent Substrate; Pierce, Rockford, IL). The quantization of phosphorylated protein expression was determined after it was normalized to corresponding total protein by measuring the optical density of respective band blots using the Quantity One software (Bio-Rad Laboratories).

KRAS and BRAF Mutational Analysis

DNA extraction was performed both on macrodissected paraffin slides, containing 80% tumor cells, and on cultured chordoma cells (1×10^6) using the QIAamp Tissue Kit (Qiagen, Hilden, Germany)

following the manufacturer's protocol. The *KRAS* gene (exons 2 and 3) was amplified using the following primers: for exon 2, forward—5'-GCC TGC TGA AAA TGA CTG AAT-3' and reverse—5'-TTA TCT GTA TCA AAG AAT GGT C-3'; for exon 3, forward—5'-GAC TGT GTT TCT CCC TTC T-3' and reverse—5'-TGG CAA ATA CAC AAA GAA AG-3'.

The *BRAF* gene (exons 11 and 15) was amplified using the following primers: for exon 11, forward—5'-TTA TTG ATG CGA ACA GTG AAT AT-3' and reverse—5'-TTA CAG TGG GAC AAA GAA TTG-3'; for exon 15, forward—5'-TCA TAA TGC TTG CTC TGA TAG GA-3' and reverse—5'-GGC CAA AAA TTT AAT CAG TGG A-3'. Briefly, DNA (100–200 ng) was amplified in a mixture containing 1× polymerase chain reaction (PCR) buffer [20 mM Tris (pH 8.3), 50 mM KCl, 1.5 mM MgCl₂], deoxyribonucleoside triphosphates (dNTPs; 200 mM each), primers (20 pM each), and 0.5 U of GoTaq polymerase (Promega, Milan, Italy) in a final volume of 25 µl. PCR conditions were given as follows: initial denaturation at 95°C for 8 minutes, followed by 35 cycles at 95°C for 40 seconds, 55°C for 40 seconds, and 72°C for 40 seconds. After visualization onto agarose gel, PCR products were treated with ExoSAP-IT (USB Corp, Cleveland, OH) following the manufacturer's protocol, amplified with BigDye Terminator version 3.1 Cycle Sequencing Kit (Applied Biosystems, Milan, Italy) using forward and reverse primers, and sequenced with an ABI PRISM 3100-Avant Genetic Analyzer (Applied Biosystems). Water was used as negative control.

Chordoma Cell Grafting and Rapamycin Treatment of Immunocompromised Mice

Experiments involving animals were approved by the Ethical Committee of the Catholic University School of Medicine (Rome, Italy). Nude athymic and non-obese diabetic–severe combined immunodeficiency (NOD-SCID) mice (males, 4–6 weeks of age; both from Charles River, Milan, Italy) were implanted subcutaneously with 1×10^6 chordoma cells at passage 10 (P10). For grafting, cells were resuspended in 0.1 ml of cold PBS, the suspension was mixed with an equal volume of cold Matrigel (BD Biosciences, Bedford, MA), and the mixture was implanted onto the right flank by subcutaneous injection using a 25-gauge needle. Only one injection was performed on a single mouse. Mice were kept under pathogen-free conditions in positive-pressure cabinets (Tecniplast Gazzada, Varese, Italy) and observed weekly for the visual appearance of tumors at injection sites. Tumor diameter was measured using a caliper, and tumor volume was calculated in mm³ according to the equation, $V = (a^2 \times b)/2$, where a is the shortest diameter and b is the longest diameter of xenografts. A group of nude athymic mice harboring chordoma xenografts was treated with rapamycin (20 mg/kg per day) [19,20]. Rapamycin (0.6 mg in 0.15 ml of saline) was injected intraperitoneally (i.p.) once daily for 4 weeks (5 days per week; total of 20 injections). Mice were maintained up to 4 weeks without any further treatment, except for measurement of tumor mass, then sacrificed with an overdose of barbiturate. Controls included mice i.p. injected with an equal volume of saline.

Histology and Immunohistochemistry of Chordoma Xenografts

Mice were deeply anesthetized and transcardially perfused with 0.1 M PBS (pH 7.4), followed by 4% paraformaldehyde in 0.1 M PBS. The implants were surgically removed and embedded in paraffin. In paraffinized sections (3-µm thick), a previous step of heat-induced antigen retrieval technique by microwave oven processing (two cycles of 5 minutes, 750 W) in citrate buffer was used. After incubation with

the primary antibody, immunodetection was performed using the avidin-biotin complex peroxidase method (Scytek) using freshly made DAB as a chromogen. For brachyury immunostaining, antigen retrieval was performed in a water bath at 100°C using 1× sodium citrate for 15 minutes. Endogenous peroxidase activity was blocked with 0.3% H₂O₂, and sections were incubated at room temperature for 1 hour with anti-brachyury antibody at a dilution of 1:50.

Results

Chordoma Cell Cultures

A chordoma cell line, herein named UCSC-CH1, was established from a tumor specimen obtained during the first staged surgical procedure. The chordoma culture was composed of two distinct cell fractions, fusiform or spindle-like cells and physaliferous cells. At early passages *in vitro* (P0–P6), the fusiform cells represented about 75% to 80% of the cell population with the remaining fraction being composed by physaliferous cells. Over time, the fusiform cells slightly outgrew the physaliferous cells and consistently accounted for 85% to 90% of the cell population at late passages. Growth curves indicated that the doubling time of the cell population was approximately 2 days (Figure W1). Up to P30, brachyury was expressed by virtually all of the cultured cells as assessed by immunohistochemistry but was strongest in the fusiform cells (Figure 2A). Unlike brachyury expression, the

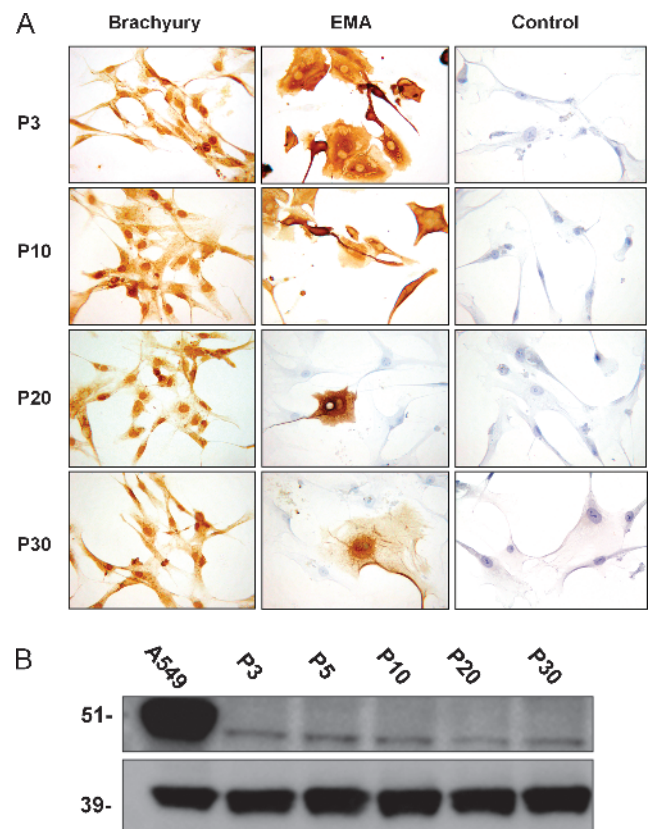


Figure 2. (A) Cultured UCSC-CH1 chordoma cells at P3 to P30. Expression of brachyury was maintained over passages. Expression of EMA consistently decreased at passages later than P10. (B) Immunoblot analysis of brachyury expression in UCSC-CH1 cells at different passages. Cell lysates of the lung carcinoma cell line A549 were used as control.

expression of EMA by the cultured chordoma cells was less uniform. At the early passages (P0–P6), EMA was highly expressed in all cells, while at late passage only 20% to 30% of the physaliferous cells maintained EMA expression, whereas the fusiform cells lost expression of EMA (Figure 2A). Western blot analysis of UCSC-CH1 chordoma cells confirmed brachyury expression that was maintained to at least P30 (Figure 2B).

In Vitro Compound Screening

To potentially identify chordoma-targeted small molecule therapies, we screened a commercially available kinase inhibitor library (Enzo Life Sciences/Biomol; <http://www.enzolifesciences.com/BML-2832/kinase-inhibitor-library>) for antiproliferative activity in the UCSC-CH1 chordoma cell line and identified two compounds, rapamycin and damnacanthal, that inhibited chordoma cell growth over a relevant concentration range with respect to their known target specificity (Figure 3, A–C). Additional compounds were antiproliferative at an initial testing concentration of 5 μ M but were subsequently determined to work through nonselective mechanisms based on a more detailed concentration response test (Table W2 and Figure W2). Such a result was expected as these kinases belong to the PI3K/Akt and KRAS/mitogen-activated protein kinase (MAPK) pathways, which have been identified as important oncogenic pathways; the PI3K/Akt pathway mediates cell survival and growth, whereas the KRAS/MAPK pathway signals cell differentiation, proliferation, and antiapoptosis.

To confirm the molecular mechanism responsible for the growth inhibition of UCSC-CH1 cells by rapamycin, we performed Western blot analysis of the mTOR pathway. Rapamycin targeting of mTOR led to a reduction of the phosphorylation state both of its upstream regulator Akt (Ser⁴⁷³) and of its downstream effector p70 S6K (Thr³⁸⁹; Figure W3).

Since chordoma has been reported in patients with tuberous sclerosis and inactivation of TSC1 and TSC2 has been suggested to play a role in chordoma development [21–24], we evaluated the state of TSC1/2 complex in UCSC-CH1 cells and its possible modulation after rapamycin treatment. In this molecular pathway, Akt negatively regulates the activity of TSC1/2 complex by TSC2 (tuberin) phosphorylation (Thr¹⁴⁶²). When TSC proteins are inactivated, mTOR is phosphorylated, thereby triggering translation, cell growth, and proliferation [24]. As shown by immunoblot with anti-phospho-tuberin/TSC2, TSC2 activity in UCSC-CH1 cells was inhibited by phosphorylation (Figure W3B). The activity of TSC1/TSC2 complex was not affected by rapamycin treatment.

Though rapamycin induced substantial growth inhibition and phospho-extracellular regulated kinase (pERK) reduction (data not shown), a fraction of chordoma cells was resistant to treatment. To potentiate rapamycin activity, we treated the UCSC-CH1 cells with a combination of rapamycin and U-0126, a MAPK pathway inhibitor. However, the combination of both compounds did not increase rapamycin-mediated cytotoxicity (Figure W4).

KRAS and BRAF Mutational Analysis

Given the sensitivity of UCSC-CH1 cells to rapamycin and the activation of the mTOR signaling pathway, we investigated the upstream oncogenes *KRAS* and *BRAF*. A heterozygous mutation at codon 12 (G12V) of *KRAS* was identified in the DNA from both patient's chordoma tissue and cultured UCSC-CH1 cells, which were assessed at P3, P12, and P30 (Figure W5). No mutations were identified in *BRAF*, exons 11 and 15.

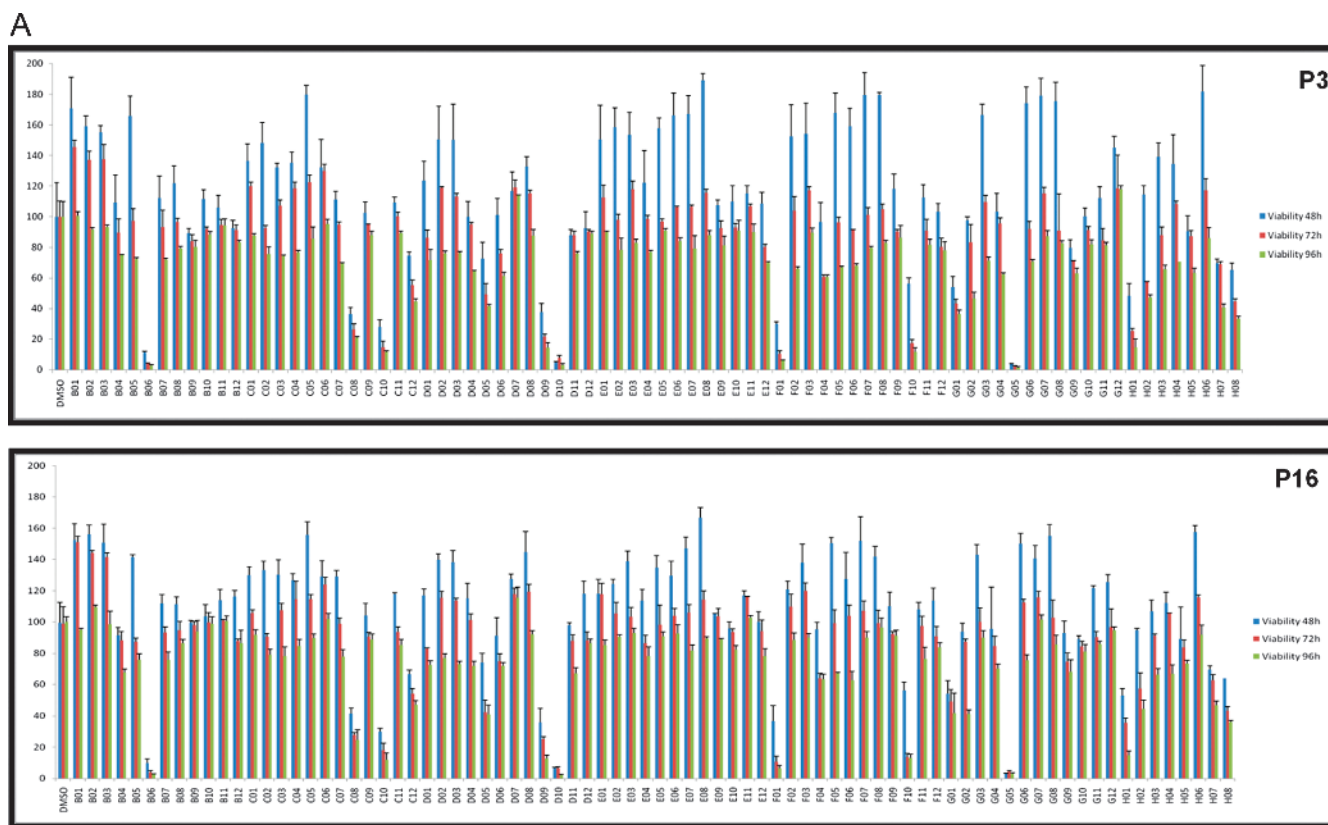
Chordoma Tumor Xenografts and Effects of Rapamycin In Vivo

Of five SCID mice that had been grafted with the UCSC-CH1 cells, three developed subcutaneous nodules that reached a mean diameter of 13 to 15 mm after 6 months (Figure 4A). The histologic pattern of the tumor xenografts strongly resembled that of the parental tumor with prominent clusters of physaliferous cells arranged in lobules or clusters embedded in a mucoid matrix (Figure 4B). Some areas of the xenografts mimicked a chondroid pattern, as demonstrated by the nuclear expression of brachyury and by the cytoplasmic expression of EMA (Figure 4B). In particular, the reduction of EMA expression by chordoma cells, which had been observed over *in vitro* passages, did not occur in the tumor xenograft.

By 4 months after grafting, subcutaneous tumors also developed in 7 of 12 nude athymic mice injected with UCSC-CH1 chordoma cells. Then, four mice received rapamycin (20 mg/kg per day *i.p.*) and three control mice were injected *i.p.* with an equal volume of saline (0.15 ml). Rapamycin was well tolerated and there was no death during 4 weeks of treatment as well as in the subsequent observational time (4 weeks). In control animals (saline injected), the tumors progressively increased in volume from 152.8 ± 6.9 mm³ (mean \pm SEM) immediately before beginning *i.p.* injection to 286.3 ± 18.4 mm³ 8 weeks later, while tumors from rapamycin-treated mice trended to reduce their volume (Figure 4, C and D). By the fourth rapamycin cycle, treated tumors were significantly smaller than control ones (107.8 ± 10.6 mm³ *vs* 224.6 ± 8.9 mm³, mean \pm SEM, $P < .001$). Upon discontinuation of rapamycin, tumors slowly regrew but remained significantly smaller than saline-treated tumors (134.7 ± 7.9 mm³ *vs* 286.3 ± 18.4 mm³, mean \pm SEM, $P < .001$; Figure 4D). Histologic examination revealed that in rapamycin-treated tumors the lobules of chordoma cells were separated by large areas consisting of dense and acellular fibrous tissue (Figure 4E). The proliferation index, as assessed by Ki-67 immunostaining, was significantly lower in rapamycin-treated tumors as compared with control tumors (5.37 ± 0.38 *vs* 3.07 ± 0.18 , mean \pm SEM, $P < .005$).

Patient Treatment with Rapamycin

Patient treatment started 1 month after the latest surgical procedure. The treatment schedule was approved by the Ethical Committee of Università Cattolica del Sacro Cuore (Rome, Italy; P/164/CE/2012). Before enrollment, the patient underwent a complete clinical evaluation, including general physical and neurologic examination, complete blood cell count, serum chemistry [serum creatinine, blood urea nitrogen (BUN), bilirubin, aspartate aminotransferase, alanine aminotransferase, alkaline phosphatase, γ -glutamyltransferase, electrolytes, glucose, cholesterol, and triglycerides], urine chemistry, cardiologic assessment, and chest roentgenogram. Sirolimus (Rapamune; Wyeth Pharmaceuticals, Havant, United Kingdom) was started at a once daily dose of 2 mg/day, taken at the same time of day either with low-fat food or without food. Dose adjustment was based on serum drug level, determined weekly for the first month and then biweekly, to maintain drug levels within a therapeutic range of 15 to 20 ng/ml [25]. Drugs interfering with cytochrome CYP3A4 were forbidden, including grapefruit juice, and treatment was planned to be discontinued in case of unacceptable toxicity. The latter was defined as the occurrence of a hematologic grade ≥ 3 adverse event or a nonhematologic grade ≥ 2 adverse event (classified according to the National Cancer Institute Common Terminology Criteria for Adverse Events, version 4.0) that did not recover after treatment interruption. General physical and



Well	Pathway	Treatment
B06	Pan-specific	Staurosporine
C08	PDGFRK	Tyrphostin 9
C10	p56 lck	Damnacanthal
C12	Src family	PP1
D05	PI 3-K	LY 294002
D09	PKC	Ro 31-8220
D10	PKC	Sphingosine
F01	ERK2, adenosine kinase, CK1, CK2,	5-Iodotubercidin
F10	PKC delta	Rottlerin
G01	EGFRK	Erbstatin analog
G02	PI 3-K	Quercetin dihydrate
G05	IKK pathway	BAY 11-7082
H01	BTK	Terreic acid
H02	Akt signaling pathway	Triciribine
H07	EGFRK	BML-265 (Erlotinib analog)
H08	mTOR	Rapamycin

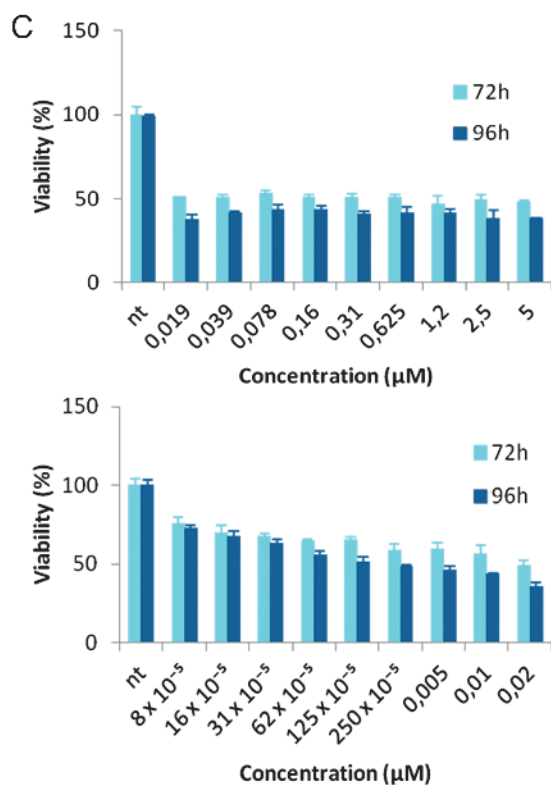


Figure 3. (A) Cell death induction by kinase Biomol inhibitors on UCSC-CH1 tested at early (P3) and late (P16) passages. Data are means \pm SD of three independent experiments. (B) List of inhibitors able to reduce UCSC-CH1 cell viability by 50% or more at 96 hours of treatment, compared to DMSO-treated control wells. (C) Titration curve of rapamycin in UCSC-CH1 at P3.

neurologic examination, complete blood cell count, and serum and urine chemistries were performed every 2 weeks. Rapamycin efficacy evaluation was based on follow-up brain MR scans. Assessment of tumor volume was performed on T2-weighted axial MR images that were retrieved from or imported into a dedicated software (Carestream Health Italia, Genova, Italy). There were no adverse events during

the 9 months of rapamycin treatment and neurologic conditions remained stable. At the 10-month follow-up MR exam, which included 9 months of rapamycin administration, the residual chordoma showed a moderate increase in size compared to the MR exam performed 1 month after surgery with the tumor volume increasing from 59.3 to 137.5 cm³ (Figure 5, A and B). However, the tumor growth rate over

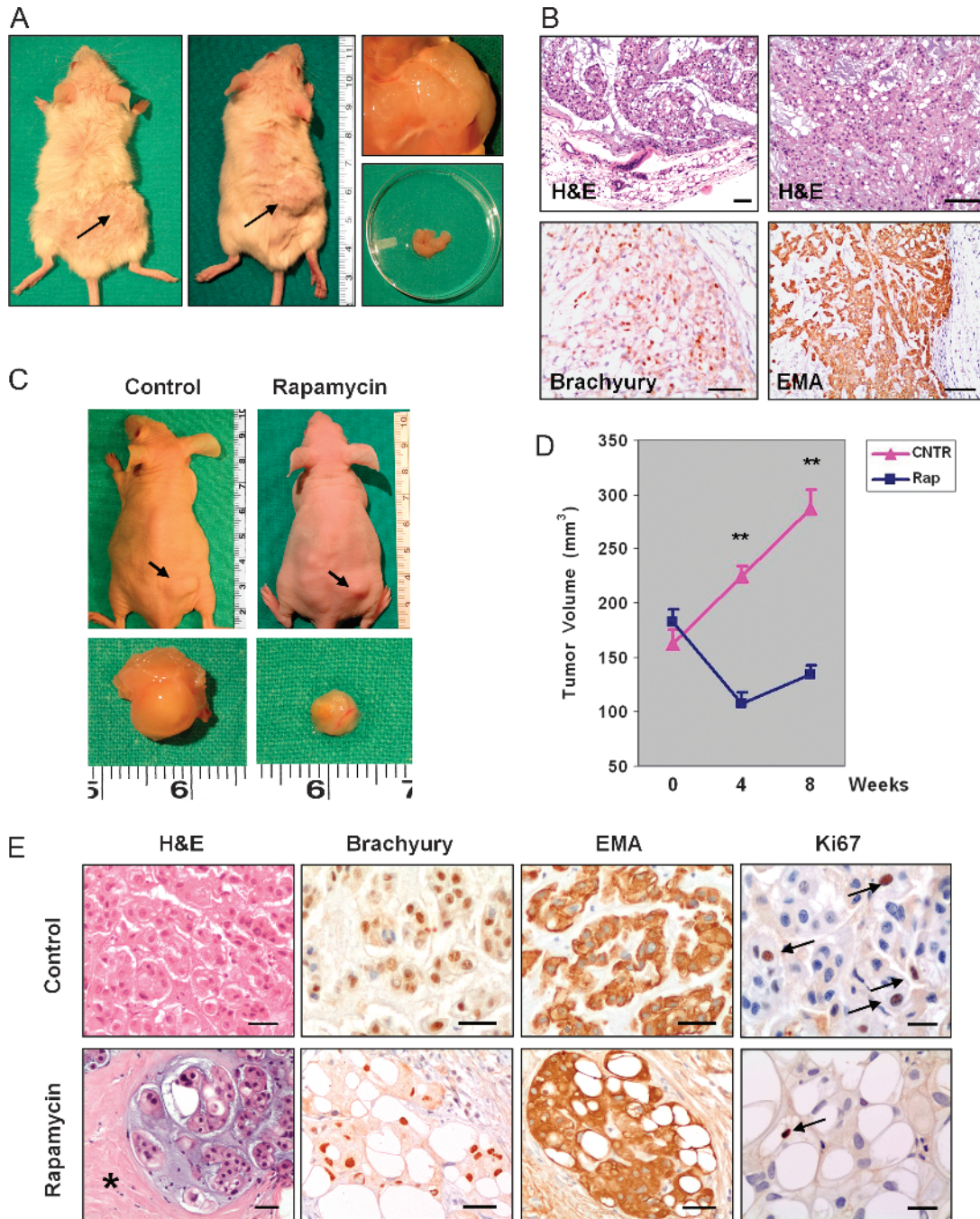


Figure 4. (A) Chordoma tumor xenografts developed 6 months after subcutaneous grafting of 1×10^6 UCSC-CH1 cells in SCID mice. (B) Histologic examination of chordoma xenografts showing lobules of physaliferous cells that express both brachyury and EMA. Scale bars, 160 μ m. (C) Chordoma tumor xenografts in control (saline-injected) and rapamycin-treated athymic mice. (D) Growth curves of chordoma xenografts in control and rapamycin-treated mice. Rapamycin was administered between week 0 and week 4 and then discontinued. $**P < .001$. (E) Histologic examination of control and rapamycin-treated chordoma xenografts. Control tumors showed the typical histologic pattern of chordoma. In rapamycin-treated xenografts, the lobules of chordoma cells were separated by large areas of amorphous tissue (asterisk). The chordoma phenotype was maintained in both groups of xenografts. Scale bars, 50 μ m in hematoxylin and eosin (H&E), brachyury, and EMA and 25 μ m in Ki-67.

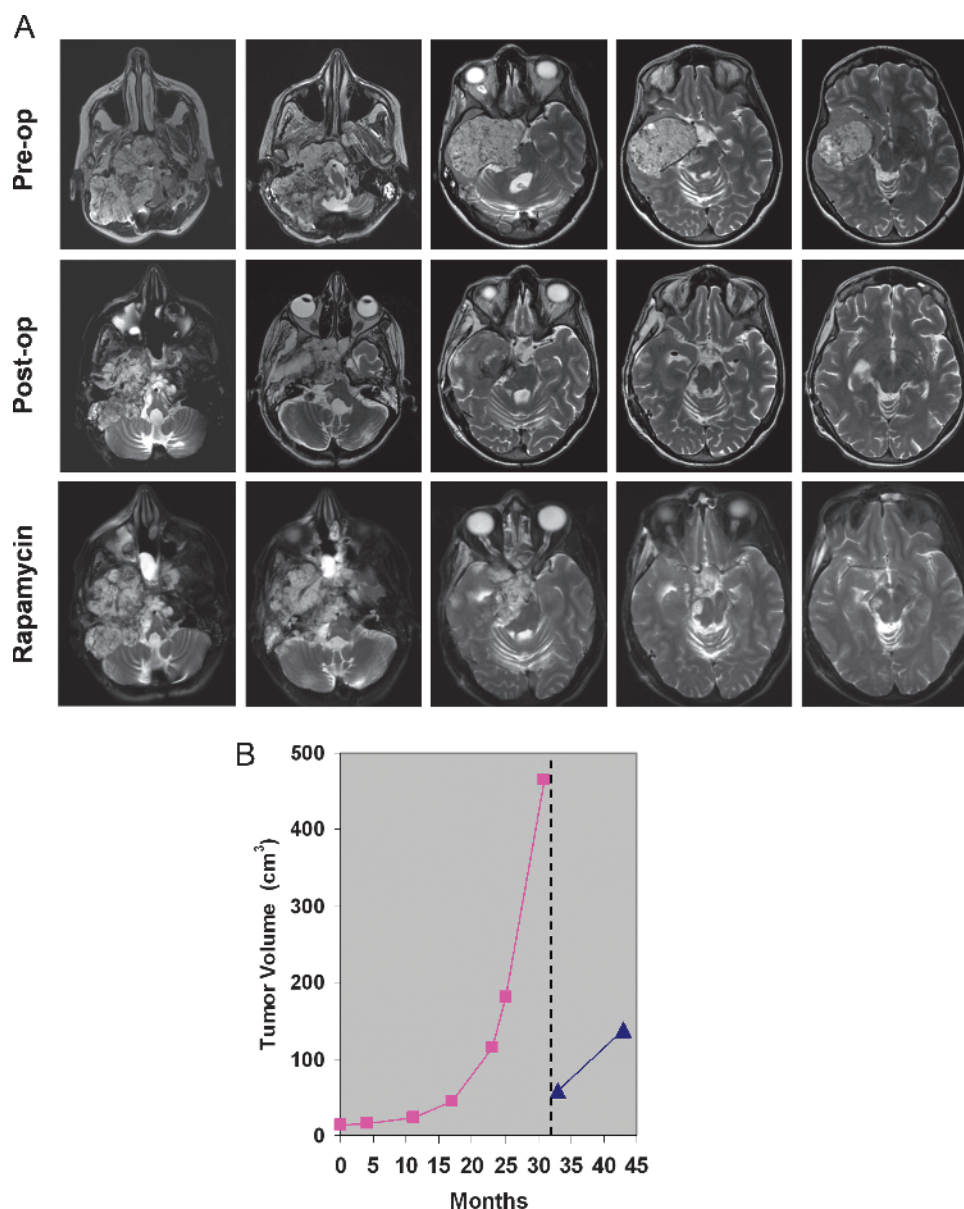


Figure 5. (A) Axial T2-weighted MR images of patient's chordoma before surgery (upper panel), 1 month after surgery before rapamycin administration (middle panel), and after 5 months of rapamycin therapy (lower panel). (B) Growth curve of patient's chordoma over 31 months before surgery (purple line) and 10 months after surgery including 9 months of rapamycin therapy (blue line).

the 10-month postoperative interval was $7.8 \text{ cm}^3/\text{month}$, that is, about 6.1-fold slower than before rapamycin therapy ($47.5 \text{ cm}^3/\text{month}$).

Discussion

The present study is unique because of the following aspects: 1) a cell line from a chordoma of the skull base has been established; 2) a targeted agent, rapamycin, has been identified that affects chordoma cell growth; 3) the efficacy of rapamycin was confirmed on an *in vivo* model; and 4) rapamycin therapy was effective in inhibiting the growth of the patient's chordoma.

In recent years, several research groups have actively been involved in establishing chordoma cell lines for preclinical research into developing effective therapies [8,10–14,16]. To date, a few cell lines have been obtained from sacral and extra-axial chordomas [10–14,16].

Chordoma of the skull base generated three long-term cell cultures in our laboratory and one primary tumor xenograft model [8,9]. In the present study, we describe establishing a cell line from a chordoma of the skull base. This cell line maintained brachyury expression at late passages *in vitro* and generated tumor xenografts in immunocompromised mice that closely mimicked the histology and phenotype of the parental tumor. Interestingly, the expression of EMA by chordoma cells, which decreased with increasing passage *in vitro*, was maintained *in vivo*, suggesting that tumor microenvironment factors influence the phenotype of chordoma cells. Using an early passage chordoma line, we performed a small molecule drug screen with a library of compounds specifically chosen for pathway inhibition and/or cytotoxic activity and designed to identify, in a short time, one or more chemotherapeutic agents that may inhibit the extremely fast-growing chordoma of our patient.

Tumor xenografts generated by injection of human chordoma cells in immunosuppressed mice require several months for their growth, representing a potential issue for translational protocols, particularly for fast-growing tumors such as the chordoma of our patient. For example, the primary human chordoma xenograft model described by Siu et al. required 5 months to grow to a size suitable for drug assessment [9]. It is important to note that the patient from whom the chordoma samples were obtained presented with tumor recurrence only 6 months after surgery [9]. Our chordoma line required 4 months to develop sizeable subcutaneous nodules and an additional 8 weeks to assess the efficacy of rapamycin *in vivo*. As previously noted [8], it is likely that chordomas generating cell lines or primary xenografts are extremely aggressive and their growth rate in the patient may be not compatible with long-lasting preclinical investigations.

Results from the small molecule screen showed that the patient-derived chordoma cells were sensitive to rapamycin, suggesting a role for the mTOR signaling pathway in chordoma growth. Han et al. have recently demonstrated that mTOR complex 1 signaling is abnormally hyperactivated in sporadic chordomas of the sacrum and that this abnormality is correlated with constitutively activated Akt likely through loss of PTEN expression [17]. These authors also reported that rapamycin at 1 nM was effective in repressing the proliferation of cultured chordoma cells [17]. Furthermore, rapamycin either alone or in combination with a PI3K inhibitor has been shown to inhibit chordoma growth in patients and to induce apoptosis in cultured sacral chordoma cells [25,26].

Our chordoma line displayed significant sensitivity to rapamycin with a significant decrease in cell number even at a concentration as low as 0.001 nM. Consistent with previous observations [17], immunohistochemical analysis demonstrated loss of PTEN expression in the chordoma cells. The mTOR pathway is frequently and constitutively activated in many types of human cancer mainly through activation of PI3K/AKT and/or inactivation of PTEN. The PI3K/AKT signaling is activated through a variety of mechanisms including mutation or amplification of cell surface receptor tyrosine kinases such as epidermal growth factor receptor (EGFR) and insulin-like growth factor receptor (IGFR), gain-of-function mutation in the *PIK3CA*, which encodes the p110 α catalytic subunit of PI3K, and loss of expression of the tumor suppressor *PTEN*, which encodes a lipid and protein phosphatase. In addition to the loss of PTEN, we found mutation of *KRAS* as a novel mechanism contributing to chordoma tumorigenesis. This mutation appears to be rare in chordomas, given that Shalaby et al. did not identify mutations of *KRAS* in 61 tumors, including sacrococcygeal, skull-based, and mobile spine chordomas [27]. Resistance of our cell line to EGFR antagonists, as assessed by our *in vitro* compound screening, is consistent with the concept that activating mutations in genes downstream of *EGFR*, like *KRAS*, represent exclusion criteria for treatment with anti-EGFR agents [28,29] and that alterations in the PI3K pathway, like *PIK3CA* gene mutations and loss of PTEN protein expression, may represent additional negative genetic regulators of EGFR-targeted therapies [30].

We are aware that a definitive demonstration of rapamycin efficacy in our patient would imply knowing, as a baseline value, the tumor growth rate after surgical resection. We attempted to determine the postoperative growth rate of chordoma tumors in cases similar to our patient by reviewing pertinent literature. Crockard et al. noted that surgically resected chordomas of the skull base show a wide distribution in their postoperative growth rate, which was assessed as tumor doubling time on follow-up MR imaging [31]. However, cases with

tumor doubling time as short as 7 months, like our patient, are expected to require additional surgery within 9 months due to clinical worsening. Although longer follow-up is warranted, over the 10-month postoperative interval, that included 9 months of rapamycin treatment, our patient did well and her neurologic improvement remained stable.

In spite of the potential advances that our approach offers for the treatment of chordoma, specifically allowing the tailoring of each protocol based on patient-derived tumor cells, some issues remain. The first concerns the loss of EMA expression by chordoma cells at passages later than P10. This phenotypic change may raise the question of the reliability of chordoma *in vitro* models. However, results of the small molecule screen performed in cells between P3 and P16 show that the loss of EMA expression does not alter sensitivity to rapamycin by cultured chordoma cells. The second issue concerns the extremely chemoresistant nature of chordoma that emerges from our *in vitro* screening. Therefore, difficulties encountered with chemotherapy for chordomas do not merely depend on the paucity of *in vitro* models but also on the intrinsic chemoresistance of this neoplasm. The third issue relates with the scarce availability for clinical research of those compounds that are the pharmaceutically active substances in herbal drugs. For example, damnacanthol, an anthraquinone compound isolated from the roots of *Morinda citrifolia* (Noni), has revealed to be highly effective in inhibiting the growth of our chordoma cell line *in vitro*. This drug has been used for traditional therapy in several chronic diseases including cancer as galenic product; however, its pharmaceutical principle is not available for treating patients. Finally, our conclusions are currently based on a small number of treated animals and on one single patient. Therefore, larger patient series as well as additional analyses, like Ki-67 staining of tumor samples from treated patients, are warranted to validate the efficacy of rapamycin in selected cases of chordoma.

References

- [1] Forsyth PA, Cascino TL, Shaw EG, Scheithauer BW, O'Fallon JR, Dozier JC, and Piegras DG (1993). Intracranial chordomas: a clinicopathological and prognostic study of 51 cases. *J Neurosurg* **78**, 741–747.
- [2] Gay E, Sekhar LN, Rubinstein E, Wright DC, Sen C, Janecka IP, and Snyderman CH (1995). Chordomas and chondrosarcomas of the cranial base: results and follow-up of 60 patients. *Neurosurgery* **36**, 887–896.
- [3] Colli BO and Al-Mefty O (2001). Chordomas of the skull base: follow-up review and prognostic factors. *Neurosurg Focus* **10**, E1.
- [4] Pallini R, Maira G, Pierconti F, Falchetti ML, Alvino E, Cimino-Reale G, Fernandez E, D'Ambrosio E, and Larocca LM (2003). Chordoma of the skull base: predictors of tumor recurrence. *J Neurosurg* **98**, 812–822.
- [5] Tzortzidis F, Elahi F, Wright D, Natarajan SK, and Sekhar LN (2006). Patient outcome at long-term follow-up after aggressive microsurgical resection of cranial base chordomas. *Neurosurgery* **59**, 230–237.
- [6] Almefty K, Pravdenkova S, Colli BO, Al-Mefty O, and Gokden M (2007). Chordoma and chondrosarcoma: similar, but quite different, skull base tumors. *Cancer* **110**, 2457–2467.
- [7] Cho YH, Kim JH, Khang SK, Lee JK, and Kim CJ (2008). Chordomas and chondrosarcomas of the skull base: comparative analysis of clinical results in 30 patients. *Neurosurg Rev* **31**, 35–43.
- [8] Ricci-Vitiani L, Pierconti P, Falchetti ML, Petrucci G, Maira G, De Maria R, Larocca LM, and Pallini R (2006). Establishing tumor cell lines from aggressive telomerase-positive chordomas of the skull base. Technical note. *J Neurosurg* **105**, 482–484.
- [9] Siu IM, Salmasi V, Orr BA, Zhao Q, Binder ZA, Tran C, Ishii M, Riggins GJ, Hann CL, and Gallia GL (2012). Establishment and characterization of a primary human chordoma xenograft model. *J Neurosurg* **116**, 801–809.
- [10] Scheil S, Brüderlein S, Liehr T, Starke H, Herms J, Schulte M, and Moller P (2001). Genome-wide analysis of sixteen chordomas by comparative genomic hybridization and cytogenetics of the first human chordoma cell line, U-CH1. *Genes Chromosomes Cancer* **32**, 203–211.

- [11] Ostroumov E and Hunter CJ (2007). The role of extracellular factors in human metastatic chordoma cell growth *in vitro*. *Spine* **32**, 2957–2964.
- [12] Ostroumov E and Hunter CJ (2008). Identifying mechanisms for therapeutic intervention in chordoma: c-Met oncoprotein. *Spine* **33**, 2774–2780.
- [13] Yang C, Hornicek FJ, Wood KB, Schwab JH, Choy E, Iafrate J, Rosenberg A, Nielsen GP, Xavier RJ, Mankin H, et al. (2010). Characterization and analysis of human chordoma cell lines. *Spine* **35**, 1257–1264.
- [14] DeComas AM, Penforis P, Harris MR, Meyer MS, and Pochampally RR (2010). Derivation and characterization of an extra-axial chordoma cell line (EACH-1) from a scapular tumor. *J Bone Joint Surg Am* **92**, 1231–1240.
- [15] Presneau N, Shalaby A, Ye H, Pillay N, Halai D, Idowu B, Tirabosco R, Whitwell D, Jacques TS, Kindblom LG, et al. (2011). Role of the transcription factor T (brachyury) in the pathogenesis of sporadic chordoma: a genetic and functional-based study. *J Pathol* **223**, 327–335.
- [16] Hsu W, Mohyeldin A, Shah SR, ap Rhys CM, Johnson LF, Sedora-Roman NI, Kosztowski TA, Awad OA, McCarthy EF, Loeb DM, et al. (2011). Generation of chordoma cell line JHC7 and the identification of Brachyury as a novel molecular target. *J Neurosurg* **115**, 760–769.
- [17] Han S, Polizzano C, Nielsen GP, Hornicek FJ, Rosenberg AE, and Ramesh V (2009). Aberrant hyperactivation of Akt and mammalian target of rapamycin complex 1 signaling in sporadic chordomas. *Clin Cancer Res* **15**, 1940–1946.
- [18] Aydemir E, Bayrak OF, Sahin F, Atalay B, Kose GT, Ozen M, Sevlı S, Dalan AB, Yalvac ME, Dogruluk T, et al. (2012). Characterization of cancer stem-like cells in chordoma. *J Neurosurg* **116**, 810–820.
- [19] Liu X, Powlas J, Shi Y, Oleksijew AX, Shoemaker AR, De Jong R, Oltersdorf T, Giranda VL, and Luo Y (2004). Rapamycin inhibits Akt-mediated oncogenic transformation and tumor growth. *Anticancer Res* **24**, 2697–2704.
- [20] Hu M, Ekshyyan O, Herman Fernandez L, Rong X, Caldito G, and Nathan CO (2011). Efficacy and comparative effectiveness of sirolimus as an anticancer drug. *Laryngoscope* **121**, 978–982.
- [21] Borgel J, Olschewski H, Reuter T, Mitterski B, and Epplen JT (2001). Does the tuberous sclerosis complex include clivus chordoma? A case report. *Eur J Pediatr* **160**, 138.
- [22] Lee-Jones L, Aligianis I, Davies PA, Puga A, Farndon PA, Stemmer-Rachamimov A, Ramesh V, and Sampson JR (2004). Sacrococcygeal chordomas in patients with tuberous sclerosis complex show somatic loss of TSC1 or TSC2. *Genes Chromosomes Cancer* **41**, 80–85.
- [23] Kimmell KT, Dayoub H, Stolzenberg ED, and Sincoff EH (2010). Chordoma in the lateral medullary cistern in a patient with tuberous sclerosis: a case report and review of the literature. *Surg Neurol Int* **1**, 13.
- [24] Diaz RJ and Cusimano MD (2011). The biological basis for modern treatment of chordoma. *J Neurooncol* **104**, 411–422.
- [25] Stacchiotti S, Marrari A, Tamborini E, Palassini E, Virdis E, Messina A, Crippa F, Morosi C, Gronchi A, Pilotti S, et al. (2009). Response to imatinib plus sirolimus in advanced chordoma. *Ann Oncol* **20**, 1886–1894.
- [26] Schwab J, Antonescu C, Boland P, Healey J, Rosenberg A, Nielsen P, Iafrate J, Delaney T, Yoon S, Choy E, et al. (2009). Combination of PI3K/mTOR inhibition demonstrates efficacy in human chordoma. *Anticancer Res* **29**, 1867–1871.
- [27] Shalaby A, Presneau N, Ye H, Halai D, Berisha F, Idowu B, Leithner A, Liegl B, Briggs TR, Bacsı K, et al. (2011). The role of epidermal growth factor receptor in chordoma pathogenesis: a potential therapeutic target. *J Pathol* **223**, 336–346.
- [28] Dalprà L, Malgara R, Miozzo M, Riva P, Volonte M, Larizza L, and Fuhrman Conti AM (1999). First cytogenetic study of a recurrent familial chordoma of the clivus. *Int J Cancer* **81**, 24–30.
- [29] Karapetis CS, Khambata-Ford S, Jonker DJ, O'Callaghan CJ, Tu D, Tebbutt NC, Simes RJ, Chalchal H, Shapiro JD, Robitaille S, et al. (2008). *K-ras* mutations and benefit from cetuximab in advanced colorectal cancer. *N Engl J Med* **359**, 1757–1765.
- [30] Molinari F, Felicioni L, Buscarino M, De Dosso S, Buttitta F, Malatesta S, Movilia A, Luoni M, Boldorini R, Alabiso O, et al. (2011). Increased detection sensitivity for *KRAS* mutations enhances the prediction of anti-EGFR monoclonal antibody resistance in metastatic colorectal cancer. *Clin Cancer Res* **17**, 4901–4914.
- [31] Crockard HA, Steel T, Plowman N, Singh A, Crossman J, Revesz T, Holton JL, and Cheeseman A (2001). A multidisciplinary team approach to skull base chordomas. *J Neurosurg* **95**, 175–183.

Table W1. List of the Library Inhibitors and Their Targets.

Well	Pathway	Treatment
B01	MEK	PD-98059
B02	MEK	U-0126
B03	p38 MAPK	SB-203580
B04	PKA, PKG, MLCK, and PKC	H-7
B05	PKA, PKG, MLCK, and PKC	H-9
B06	Pan-specific	Staurosporine
B07	EGFRK, PDGFRK	AG-494
B08	HER1-2	AG-825
B09	EGFRK	Lavendustin A
B10	EGFRK	RG-14620
B11	EGFRK	Tyrphostin 23
B12	EGFRK	Tyrphostin 25
C01	EGFRK, PDGFRK	Tyrphostin 46
C02	EGFRK	Tyrphostin 47
C03	EGFRK	Tyrphostin 51
C04	Negative control for tyrosine kinase inhibitors	Tyrphostin 1
C05	Tyrosine kinases	Tyrphostin AG 1288
C06	EGFRK	Tyrphostin AG 1478
C07	Tyrosine kinases	Tyrphostin AG 1295
C08	PDGFRK	Tyrphostin 9
C09	IRK	Hydroxy-2-naphthalenylmethylphosphonic acid
C10	p56 lck	Damnacanthal
C11	Syk	Piceatannol
C12	Src family	PP1
D01	JAK-2	AG-490
D02	IRAK	AG-126
D03	PDGFRK	AG-370
D04	NGFRK	AG-879
D05	PI3K	LY 294002
D06	PI3K	Wortmannin
D07	PKC	GF 109203X
D08	PKC	Hypericin
D09	PKC	Ro 31-8220
D10	PKC	Sphingosine
D11	PKA	H-89
D12	PKA, PKG	H-8
E01	PKA, PKG	HA-1004
E02	PKA, PKG	HA-1077
E03	EGFRK, CaMK II	2-Hydroxy-5-(2,5-dihydroxybenzylamino)benzoic acid
E04	CaMK II	KN-62
E05	CaMK II	KN-93
E06	MLCK	ML-7
E07	MLCK	ML-9
E08	p58 PITSLRE β 1	2-Aminopurine

Table W1. (continued)

Well	Pathway	Treatment
E09	CDK	N9-isopropyl-olomoucine
E10	CDK	Olomoucine
E11	Negative control for olomoucine	iso-olomoucine
E12	CDK	Roscovitine
F01	ERK2, adenosine kinase, CK1, CK2,	5-Iodotubercidin
F02	BTk	LFM-A13
F03	p38 MAPK	SB-202190
F04	Src family	PP2
F05	CRAF	ZM 336372
F06	Flk1	SU 4312
F07	PDGFRK	AG-1296
F08	CRAF	GW 5074
F09	PKC	Palmitoyl-DL-carnitine Cl
F10	PKC δ	Rottlerin
F11	Tyrosine kinases	Genistein
F12	Negative control for genistein	Daidzein
G01	EGFRK	Erbstatin analog
G02	PI3K	Quercetin dihydrate
G03	Flk1	SU1498
G04	JAK-3	ZM 449829
G05	IKK pathway	BAY 11-7082
G06	CK II	5,6-Dichloro-1-B-D-ribofuranosylbenzimidazole
G07	PKC α , PKC γ	2,2',3,3',4,4'-Hexahydroxy-1,1'-biphenyl-6,6'-dimethanol dimethyl ether
G08	JNK	SP 600125
G09	GSK-3 β , CDK5	Indirubin
G10	GSK-3 β	Indirubin-3'-monoxime
G11	ROCK	Y-27632
G12	GSK-3 β	Kenpaullone
H01	BTk	Terreic acid
H02	Akt signaling pathway	Triciribine
H03	Akt	BML-257
H04	IKK2	SC-514
H05	Cdk5/p25	BML-259
H06	CK-II	Apigenin
H07	EGFRK	BML-265 (erlotinib analog)
H08	mTOR	Rapamycin

BTk indicates Bruton agammaglobulinemia tyrosine kinase; CaMK II, calmodulin-dependent protein kinase II; EGFRK, epidermal growth factor receptor kinase; HER1-2, human epidermal growth factor receptor 1-2; IKK2, inhibitor of nuclear factor kappa-B kinase 2; IRAK, interleukin receptor-associated kinase; IRK, insulin receptor kinase; JAK-2, Janus kinase 2; MEK, mitogen-activated protein kinase kinase; MLCK, myosin light chain kinase; NGFRK, nerve growth factor receptor kinase; PDGFRK, platelet-derived growth factor receptor-associated tyrosine kinase; PKA, cAMP-dependent protein kinase; PKC, protein kinase C; PKG, cGMP-dependent protein kinase.

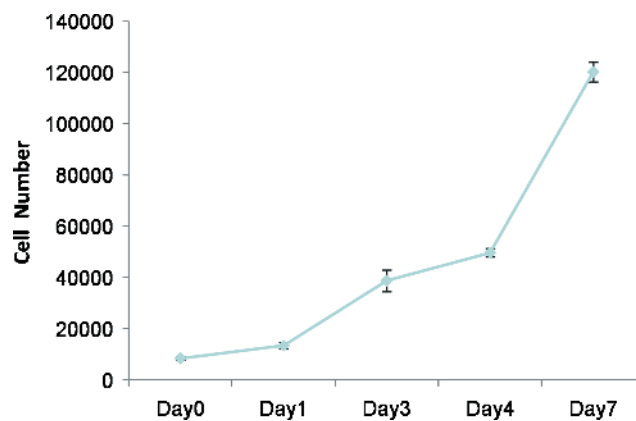


Figure W1. Growth curve of UCSC-CH1 at P4. Data are means \pm SD of three independent experiments.

Table W2. IC₅₀ Values of Compounds Active against UCSC-CH1 Chordoma Cell Line.

Treatment	IC ₅₀
Quercetin dihydrate	5.948562953
BML-265	4.43136049
PP1	4.377361764
LY249002	3.606772465
Triciribine	3.339349257
Erbastin analog	2.906892452
Terreic acid	2.793404793
Tyrphostin 9	2.588057899
Sphingosine	2.538831986
5-Iodotubercin	2.260229722
BAY 11-7082	2.112517096
Rottlerin	2.016850515
Damnacanthal	0.03
Rapamycin	0.007031962

IC₅₀ indicates 50% inhibitory concentration.

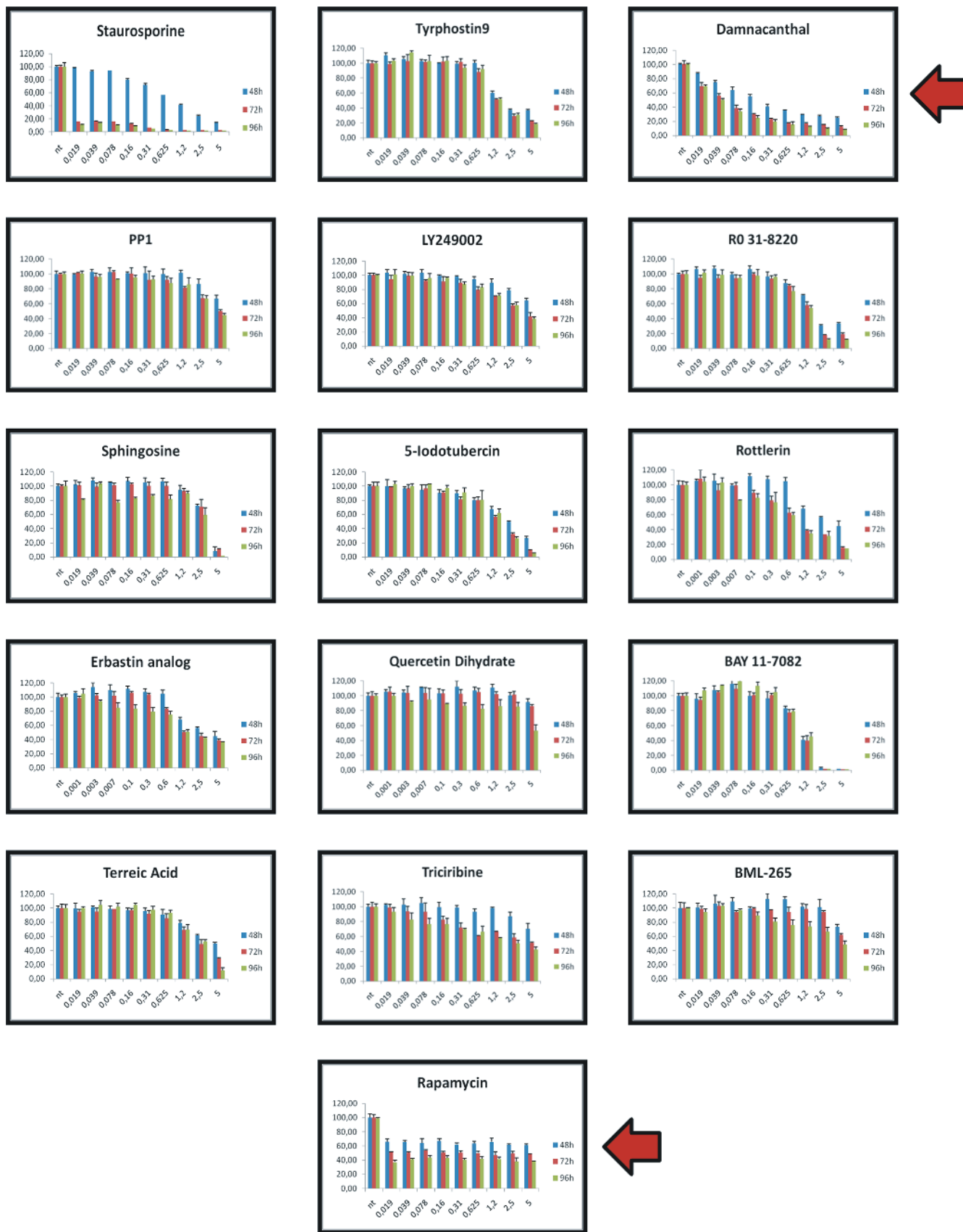


Figure W2. Titration curves of the 15 selected compounds at 48, 72, and 96 hours after treatment. Staurosporine was used as control.

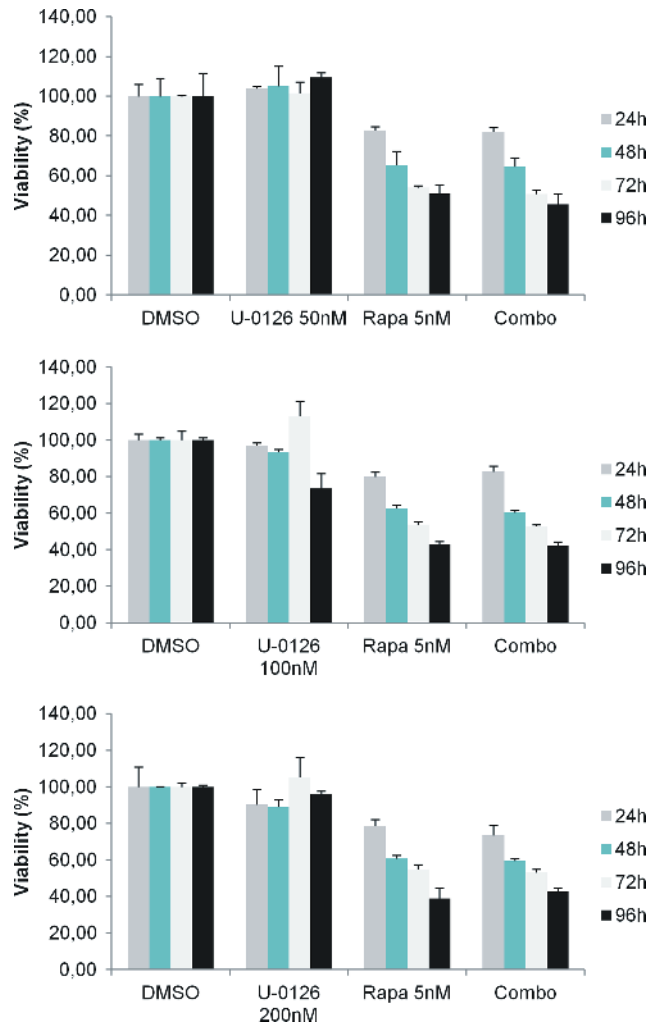
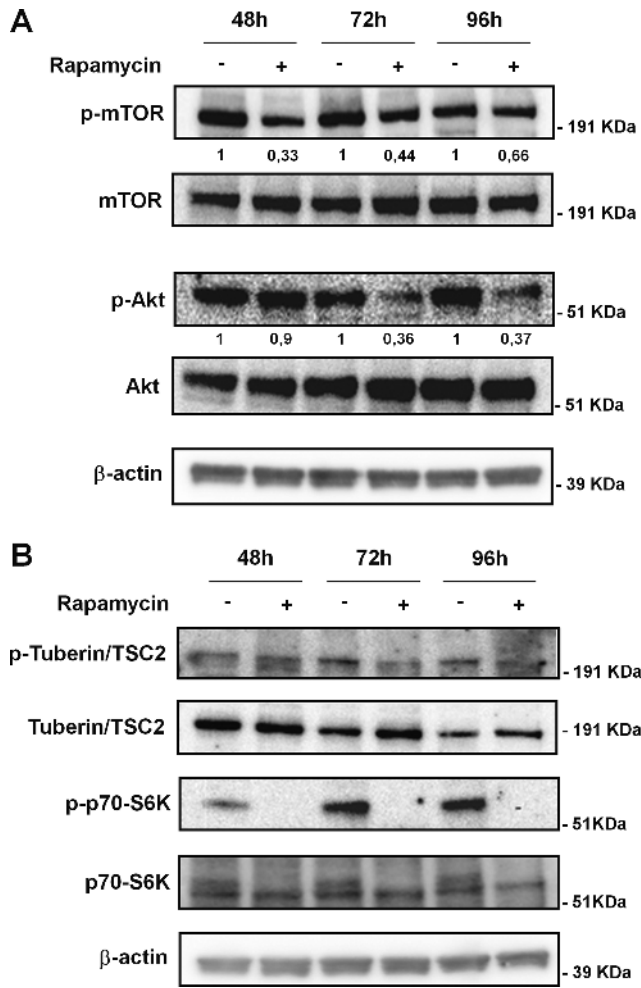


Figure W3. Effect of rapamycin treatment (5 nM; 48, 72, and 96 hours) on phospho-mTOR and phospho-Akt (A) and on phospho-TSC2 and phospho-p70 S6K (B). Numbers indicate the ratio of the phosphorylated protein normalized to the amount of corresponding total protein.

Figure W4. MAPK pathway inhibition does not increase rapamycin-mediated cytotoxicity. Effect of rapamycin (Rapa; 5 nM), U-0126 (50, 100, 200 nM) or the combination of both compounds on cell viability after 24, 48, 72, and 96 hours of treatment. Error bars indicate SD.

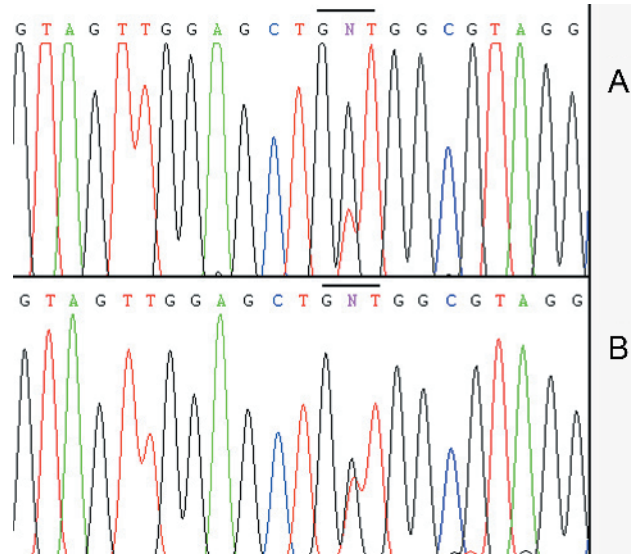


Figure W5. The figure shows a fragment of the *KRAS* sequence (from nucleotide 22 to nucleotide 44) from patient's chordoma tissue (A) and UCSC-CH1 chordoma cells at P12 (B). Both samples show a heterozygous mutation of codon 12 (bar line) with a change of GGT to GTT. This mutation determines the substitution of a glycine with a valine amino acid (G12V).